High-Fidelity Initial Models for Neutron Star Simulations

Matthias Raives
Mentors: Christian Ott & Mark Scheel

November 1, 2013

Abstract

Precision predictions of gravitational waves from pulsating and merging neutron stars rely on numerical relativity simulations, which, in turn, rely on physically and numerically accurate initial conditions. Specialized codes called initial data solvers are used to numerically integrate the general relativity and hydrodynamics equations to determine the matter and spacetime properties in and around the star. The current single star initial data solver used by our group, CST, is of limited accuracy; we would require a different code if we desired more accurate models. To that end, we have investigated two different initial data solvers in order to determine their suitability as a replacement for CST. These codes are evaluated against each other and against CST by the degree to which they satisfy several constraints, most notably a virial identity (GRV2) which vanishes for axisymmetric, stationary, and asymptotically flat spacetime, conditions which are met for single star models. Future work will entail comparing the different initial data solvers for binary stars and evolving single and binary star models in neutron star evolution code.

Contents

1 Introduction **1**
1.1 Motivation . . . 1
1.2 Spectral Methods . . . 2
1.3 GRV2 . . . 2

2 Initial Data Solvers **3**
2.1 AKM Solver . . . 3
2.1.1 Spectral Coordinates . . . 3
2.1.2 GRV2 in the AKM Spectral Domain . . . 4
2.1.3 Boundary Behavior in the Exterior Subdomain . . . 5
2.2 LORENE . . . 5

3 Results **5**

A Boundary Behavior in the Exterior Subdomain **8**
A.1 $s = 0$ Limit . . . 8
A.2 $s = 1$ Limit . . . 8
A.3 t Limits . . . 9

1 Introduction

1.1 Motivation

Neutron star binaries and their mergers are expected to be a primary source of detectable gravitational waves. While our current neutron star binary simulations converge to higher precision than LIGO or Advanced LIGO can detect, increased precision will be of great benefit to next-generation gravitational wave

detectors. Furthermore, increased precision will give us the ability to better study the effect that introducing microphysics has on our models.

Out current initial data solver, CST [1, 2] is limited in precision to approximately 1 part in 10^3. Increased precision for the initial data solver is required to increase the precision of the simulation as a whole, as the time-evolution code introduces additional numerical error with each time step. Furthermore, lack of precision in the initial data solver makes it difficult to diagnose the sources of error possibly in the time-evolution code and improve the time-evolution code in general.

1.2 Spectral Methods

Spectral methods are methods used to solve differential equations, in which functions are represented by high order polynomials. In spectral methods, a function $f(x) : \mathbb{R} \mapsto \mathbb{R}$ is represented by an interpolating polynomial $I(x)$ (in the domain $[-1, 1]$). The interpolating polynomial is equal to $f(x)$ on a set of points X called the grid. These grid points are usually chosen such that they correspond to the zeroes or extrema of an appropriate Chebychev polynomial. The problem is thus reduced to determining the coefficients of the interpolating polynomial and numerically integrating and differentiating a polynomial [3].

An important part of spectral methods is the idea of compactified domains. A compactified domain is an infinite domain such as $[0, \infty)$ that is mapped to a finite domain such as $[0, 1]$. The primary advantage of compactified domains is that they allow the use of boundary conditions at infinity in numerical schemes. They also provide additional accuracy for integrals that extend to infinity.

1.3 GRV2

GRV2 [4] is a virial identity which holds in asymptotically flat, axisymmetric spacetime. It is thus particularly useful to check the accuracy of single star simulations. We intended to use it as a quantitative measure of the accuracy of various initial data solvers.

With a metric of the form[1]

$$\mathrm{d}s^2 = -e^{2\nu}\mathrm{d}t^2 + e^{2\alpha}(\mathrm{d}\varrho^2 + \mathrm{d}\zeta^2) + B^2\varrho^2 e^{-2\nu}(\mathrm{d}\varphi - \omega\,\mathrm{d}t)^2 \tag{1}$$

where (ν, ω, α, B) are the metric potentials, GRV2 can be expressed as [5, 6]:

$$\text{GRV2} = |1 - \lambda_2| = 0 \tag{2}$$

$$\lambda_2 = 8\pi \frac{\int_0^{+\infty}\int_0^{+\infty} f(\varrho,\zeta)\,\mathrm{d}\varrho\,\mathrm{d}\zeta}{\int_0^{+\infty}\int_0^{+\infty} g(\varrho,\zeta)\,d\varrho\,d\zeta} \tag{3}$$

$$f(\varrho,\zeta) = \left(p + (\varepsilon + p)\frac{v^2}{1-v^2}\right)e^{2\alpha} \tag{4}$$

$$g(\varrho,\zeta) = (\nabla\nu)^2 - \frac{3}{4}\varrho^2 B^2 e^{-4\nu}(\nabla\omega)^2 \tag{5}$$

$$(\nabla\alpha)^2 \equiv \left(\frac{\partial\alpha}{\partial\varrho}\right)^2 + \left(\frac{\partial\alpha}{\partial\zeta}\right)^2 \tag{6}$$

As a virial identity, GRV2 expresses a relationship between the equilibrium states of the different forms of energy in the rotating neutron star. In the Newtonian limit, GRV2 becomes:

$$\int_0^{\pi}\int_0^{\infty}\left[p + \rho v^2 - \frac{1}{8\pi G}(\nabla\nu)^2\right] r\,\mathrm{d}r\,\mathrm{d}\theta = 0 \tag{7}$$

with the integral taken in spherical coordinates. This roughly corresponds to the standard virial theorem relating rotational (the ρv^2 term), gravitational (the $(8\pi G)^{-1}(\nabla\nu)^2$ term), and thermal (the p term) energies in a bound system.

[1] I've written GRV2 here with the metric used by the AKM solver, though in principle other metrics (i.e., other choices of metric potentials) can be used.

2 Initial Data Solvers

2.1 AKM Solver

The AKM solver [7, 5] uses a two domain spectral method. Physical space (in cylindrical (ϱ, ζ) coordinates) is broken up into two subdomains, each mapped to the cross product of intervals ($[0,1] \times [0,1]$ in spectral (s,t) space) where the outer subdomain is compactified. The AKM solver uses the domain $[0,1]$ instead of $[-1,1]$ because it assumes the star to be equatorially as well as axially symmetric. The boundary between subdomains is placed at the stellar surface; this allows for smooth representations of the physical fields, eliminating the Gibbs phenomenon across the surface.

Physically, the AKM solver treats a rotating star as an axisymmetric, perfect fluid with stress energy tensor

$$T_{\alpha\beta} = (\epsilon + p) u_\alpha u_\beta + p g_{\alpha\beta} \tag{8}$$

where ϵ is the total energy density, p is the pressure, and u_i is the matter four-velocity. Here $\epsilon = \rho_o + \rho_i$, where ρ_o is the rest energy density and ρ_i is the internal energy density.

The AKM solver uses a Newton-Raphson scheme to iteratively solve the nonlinear GR and hydrodynamic equations for all field quantities and the shape of the stellar surface. It then integrates quantities such as the gravitational and baryon mass and the total angular momentum.

2.1.1 Spectral Coordinates

The AKM solver uses a different set of coordinates in each spectral subdomain. Each subdomain is formally indicated with an index k. In the interior ($k = 1$) subdomain, the mapping

$$\begin{aligned} \varrho_1^2(s,t) &= r_e^2 t \\ \zeta_1^2(s,t) &= s\left(G(t) - r_e^2 t\right) \end{aligned} \tag{9}$$

is used. The inner domain is bounded by

$$\begin{aligned} &s = 0 : \text{equatorial plane, } \zeta = 0 \\ &s = 1 : \text{stellar surface, } (\varrho, \zeta) = \left(r_e\sqrt{t}, \sqrt{G(t) - r_e^2 t}\right) \\ &t = 0 : \text{rotation axis, } \varrho = 0 \\ &t = 1 : \text{equator, } \varrho = r_e, \zeta = 0. \end{aligned}$$

In the exterior ($k = 0$) subdomain, the mapping

$$\begin{aligned} \varrho_0^2(s,t) &= t\left(r_e^2 - r_p^2 + \xi^2(s)\right) \\ \zeta_0^2(s,t) &= (1-t)\left(\xi^2(s) - r_p^2\right) + G(t) - r_e^2 t \end{aligned} \tag{10}$$

with

$$\xi(s) = r_p + r_e \frac{1 - \sigma(s)}{\sigma(s)} \tag{11}$$

$$\sigma(s) = \frac{\sinh\left((1-s)\ln\epsilon_s\right)}{\sinh\left(\ln\epsilon_s\right)} \tag{12}$$

is used. The outer domain is bounded by

$$\begin{aligned} &s = 0 : \text{spatial infinity, } \sqrt{\varrho^2 + \zeta^2} \to \infty \\ &s = 1 : \text{stellar surface} \\ &t = 0 : \text{rotation axis, } \varrho = 0 \\ &t = 1 : \text{equatorial plane, } \zeta = 0. \end{aligned}$$

In both domains, r_e and r_p are the equatorial and polar radii of the star. $G(t)$ is a one dimensional function, $G : [0, 1] \to \mathbb{R}$, which describes the shape of the stellar surface. In particular, $G(0) = r_p^2$ and $G(1) = r_e^2$. The parameter ϵ_s is a free parameter which can be rescaled to adjust the resolution of the spatial mesh in the vicinity of the stellar surface [5]. This is primarily useful for highly flattened stars; in typical cases, we set $\epsilon_s = 1$ which results in $\sigma(s) = s$.

2.1.2 GRV2 in the AKM Spectral Domain

For accurate computation of GRV2, we must compute it in the spectral domain. Thus, we necessarily must split up the integrals in (3) into their interior and exterior subdomain parts:

$$\lambda_2 = 8\pi \frac{\int_0^1 \int_0^1 f_0(s,t)|\mathbf{J}_0| \,\mathrm{d}s \,\mathrm{d}t + \int_0^1 \int_0^1 f_1(s,t)|\mathbf{J}_1| \,\mathrm{d}s \,\mathrm{d}t}{\int_0^1 \int_0^1 g_0(s,t)|\mathbf{J}_0| \,\mathrm{d}s \,\mathrm{d}t + \int_0^1 \int_0^1 g_1(s,t)|\mathbf{J}_1| \,\mathrm{d}s \,\mathrm{d}t}. \tag{13}$$

We note that $f(s,t)$ is uniformly 0 in the exterior subdomain, as all matter terms are necessarily zero outside the star:

$$\lambda_2 = 8\pi \frac{\int_0^1 \int_0^1 f_1(s,t)|\mathbf{J}_1| \,\mathrm{d}s \,\mathrm{d}t}{\int_0^1 \int_0^1 g_0(s,t)|\mathbf{J}_0| \,\mathrm{d}s \,\mathrm{d}t + \int_0^1 \int_0^1 g_1(s,t)|\mathbf{J}_1| \,\mathrm{d}s \,\mathrm{d}t}. \tag{14}$$

Here, $|\mathbf{J}_0|$ and $|\mathbf{J}_1|$ are the determinants of the Jacobian of the transformation from (ϱ, ζ) space into (s,t) space in domains 0 and 1, respectively. Thus we see:

$$|\mathbf{J}_1| = \frac{1}{4\varrho_1\zeta_1}\left(\frac{\mathrm{d}\varrho_1^2}{\mathrm{d}t}\frac{\mathrm{d}\zeta_1^2}{\mathrm{d}s}\right) = \frac{r_e\left(G(t) - r_e^2 t\right)^{1/2}}{4(st)^{1/2}} \tag{15}$$

and[2]

$$|\mathbf{J}_0| = \frac{1}{4\varrho_0\zeta_0}\left(\frac{\mathrm{d}\varrho_0^2}{\mathrm{d}s}\frac{\mathrm{d}\zeta_0^2}{\mathrm{d}t} - \frac{\mathrm{d}\varrho_0^2}{\mathrm{d}t}\frac{\mathrm{d}\zeta_0^2}{\mathrm{d}s}\right). \tag{16}$$

The nabla operator also takes a different form in (s,t) space:

$$(\nabla_{st}\alpha)^2 = 4\left(\varrho_k^2\left(\frac{\partial\alpha}{\partial s}\frac{\partial s}{\partial\varrho_k^2} + \frac{\partial\alpha}{\partial t}\frac{\partial t}{\partial\varrho_k^2}\right)^2 + \zeta_k^2\left(\frac{\partial\alpha}{\partial s}\frac{\partial s}{\partial\zeta_k^2} + \frac{\partial\alpha}{\partial t}\frac{\partial t}{\partial\zeta_k^2}\right)^2\right). \tag{17}$$

Note that, in the outer domain, the derivatives such as $\partial s/\partial\varrho_k^2$ cannot be determined from the coordinate definitions in (10). Instead, we use the fact that the Jacobian of the inverse transformation is equal to the inverse of the Jacobian of the original transformation to show that

$$\begin{aligned}
\frac{\partial s}{\partial\varrho_k^2} &= \left(\frac{\mathrm{d}\varrho_k^2}{\mathrm{d}s}\frac{\mathrm{d}\zeta_k^2}{\mathrm{d}t} - \frac{\mathrm{d}\varrho_k^2}{\mathrm{d}t}\frac{\mathrm{d}\zeta_k^2}{\mathrm{d}s}\right)^{-1}\frac{\partial\zeta_k^2}{\partial t} \\
\frac{\partial s}{\partial\zeta_k^2} &= -\left(\frac{\mathrm{d}\varrho_k^2}{\mathrm{d}s}\frac{\mathrm{d}\zeta_k^2}{\mathrm{d}t} - \frac{\mathrm{d}\varrho_k^2}{\mathrm{d}t}\frac{\mathrm{d}\zeta_k^2}{\mathrm{d}s}\right)^{-1}\frac{\partial\varrho_k^2}{\partial t} \\
\frac{\partial t}{\partial\varrho_k^2} &= -\left(\frac{\mathrm{d}\varrho_k^2}{\mathrm{d}s}\frac{\mathrm{d}\zeta_k^2}{\mathrm{d}t} - \frac{\mathrm{d}\varrho_k^2}{\mathrm{d}t}\frac{\mathrm{d}\zeta_k^2}{\mathrm{d}s}\right)^{-1}\frac{\partial\zeta_k^2}{\partial s} \\
\frac{\partial t}{\partial\zeta_k^2} &= \left(\frac{\mathrm{d}\varrho_k^2}{\mathrm{d}s}\frac{\mathrm{d}\zeta_k^2}{\mathrm{d}t} - \frac{\mathrm{d}\varrho_k^2}{\mathrm{d}t}\frac{\mathrm{d}\zeta_k^2}{\mathrm{d}s}\right)^{-1}\frac{\partial\varrho_k^2}{\partial s}.
\end{aligned} \tag{18}$$

Thus we can write

$$(\nabla_{st}\alpha)^2 = (2\varrho_k\zeta_k)^{-2}|\mathbf{J}_k|^{-2}\left(\varrho_k^2\left(\frac{\partial\alpha}{\partial s}\frac{\partial\zeta_k^2}{\partial t} - \frac{\partial\alpha}{\partial t}\frac{\partial\zeta_k^2}{\partial s}\right)^2 + \zeta_k^2\left(\frac{\partial\alpha}{\partial s}\frac{\partial\varrho_k^2}{\partial t} - \frac{\partial\alpha}{\partial t}\frac{\partial\varrho_k^2}{\partial s}\right)^2\right), \tag{19}$$

which holds in either subdomain.

[2]The ϱ_0 and ζ_0 derivatives are not expanded in order to save space.

2.1.3 Boundary Behavior in the Exterior Subdomain

The integrand $g_0(s,t)$ (the exterior subdomain portion of $g(\varrho,\zeta)$ in (s,t) space) does not behave nicely at the $s=0,\ t=0,\ t=1$ boundaries. Much of the erratic behavior is due to the $(\varrho\zeta)^{-1}$ term, which causes problems as ϱ or ζ tend to 0. Specifically, the integrand goes to infinity at certain boundaries, while at others, the numerator and denominator both tend towards 0 or infinity. As we know a priori that the integral should be finite, we must take additional care in evaluating the integral and integrand at the boundaries. Creative choices of differentials can eliminate some of the erratic boundary behavior. Integrating over $\mathrm{d}\sqrt{t}$, for example[3], we find:

$$\begin{aligned}\lim_{t\to 0} g_0(s,t)|\mathbf{J}_0|\sqrt{t} &= 4s\sqrt{\frac{-2r_p(s-1)s + r_e(1+2(s-1)s)}{r_e}}\left(\frac{\partial\nu}{\partial s}\right)^2 \\ \lim_{t\to 1} g_0(s,t)|\mathbf{J}_0|\sqrt{t} &= \infty\end{aligned} \tag{20}$$

whereas neither of these limits are finite when integrating over $\mathrm{d}t$. Some of the problems in these integrals may be solved by integrating $g_0(s,t)$ term by term and possibly using a different choice of differential for each term.

The $s\to 0$ limit can be evaluated when integrating over $\mathrm{d}s$:

$$\lim_{s\to 0} g_0(s,t)|\mathbf{J}_0| = 0 \tag{21}$$

and the integrand behaves nicely as $s\to 1$. The s and t limits are done in detail in Appendix A.

2.2 LORENE

LORENE [8] is a library of C++ classes useful for numerical and computational astrophysics, though it can be used for any problem solvable by multi-domain spectral methods. It implements classes for mathematical structures such as vector, matrices, and tensors, as well as astrophysical structures such as stars.

Various codes have been built using LORENE and come distributed with the LORENE source, including one designed for rotating stars. This code uses a multi-domain spectral method, where the number of subdomains is greater than 2. The subdomains are constructed such that there is a boundary on the stellar surface, allowing the code to avoid the Gibbs phenomenon as in the AKM solver. The code also has angular domain boundaries. Physically, the LORENE code models a rotating star much like the AKM solver.

I did not get far enough in my work with the AKM solver to begin studying LORENE codes in detail; I include it here for the sake of completeness as it was the primary code to be compared to the AKM solver.

3 Results

I have yet to obtain results that satisfy the primary goals of the project, to determine whether LORENE or the AKM solver is a better replacement for CST as our groups initial data solver. However, I intend to continue work on this project and thus I hope to be able to have a definitive answer in due course.

I do however have preliminary results outlining the convergence of various parameters in the AKM solver (when calculated in the spectral domain) and the convergence of GRV2 using a second order Simpson's Rule method in the AKM solver's pseudo-Cartesian output grid (this is very inaccurate as GRV2 depends on values which are nonzero in regions extending to spatial infinity). These are outlined in figure 1. In plot axis labels, "Difference" indicates that self-convergence is used, and the data point for quantity Q for n spectral coefficients, is reported as

$$|Q_n - Q_{22}|$$

that is, the magnitude of the difference in the value of Q calculated for n spectral coefficients and the value of Q calculated for $n = n_{max} = 22$ spectral coefficients.

[3] Integrating over $\mathrm{d}\sqrt{t}$ causes an additional factor of $\sqrt{t}$ to appear in the numerator.

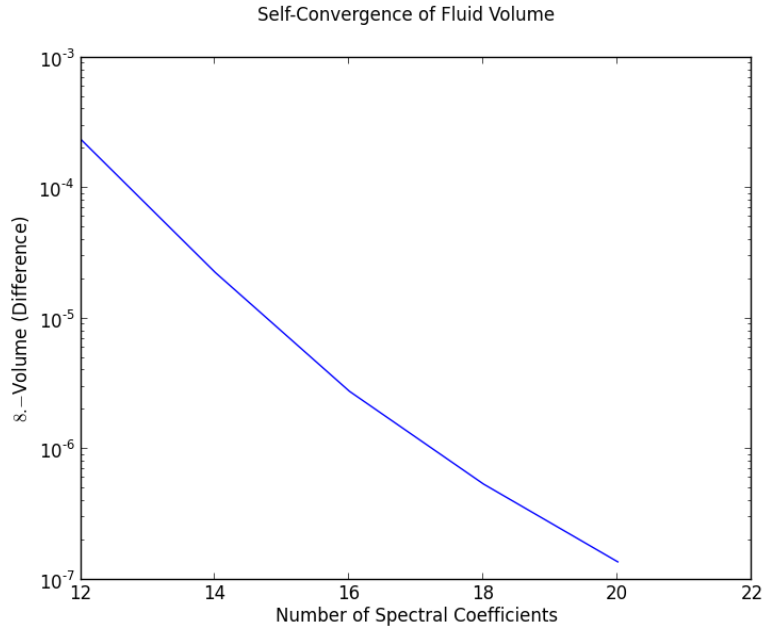

(a)

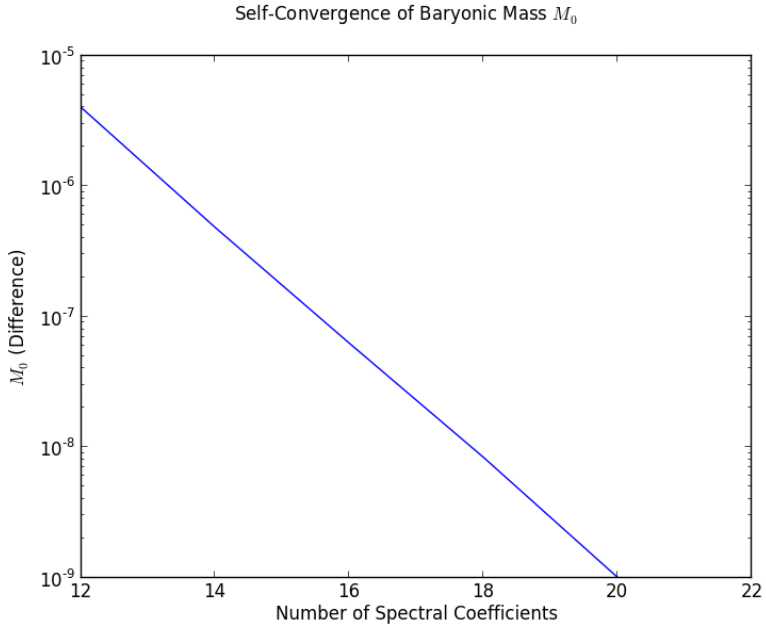

(b)

Figure 1. (a) Self-convergence of the volume of the neutron star in the AKM solver for increasing number of spectral coefficients. Here, a non-rotating neutron star of radius $r = 2$ is was used, and volume was scaled by a factor of $\frac{3}{4\pi}$. The scaled volume at n spectral coefficients, V_n was subtracted from the expected scaled volume of 8 before taking the difference with V_{22}. **(b)** Self-convergence of the baryon mass of the neutron star in the AKM solver for increasing number of spectral coefficients.

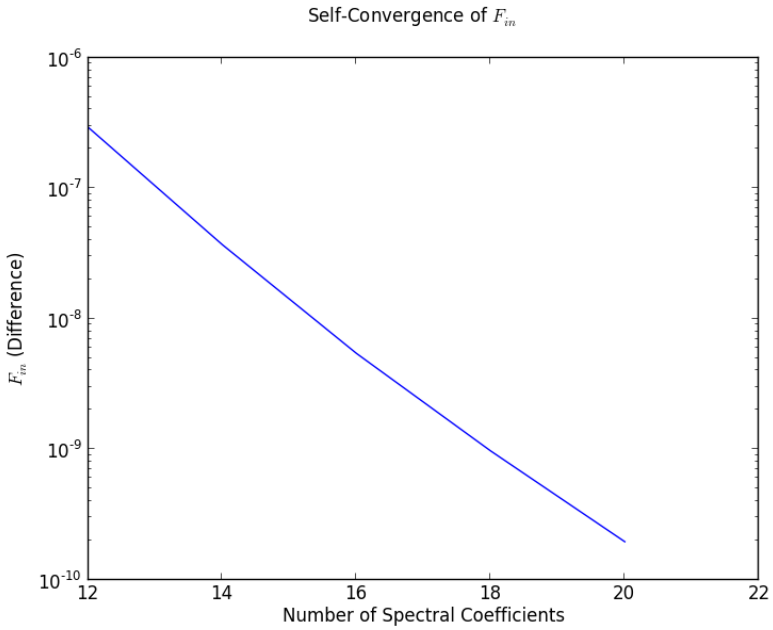

(c)

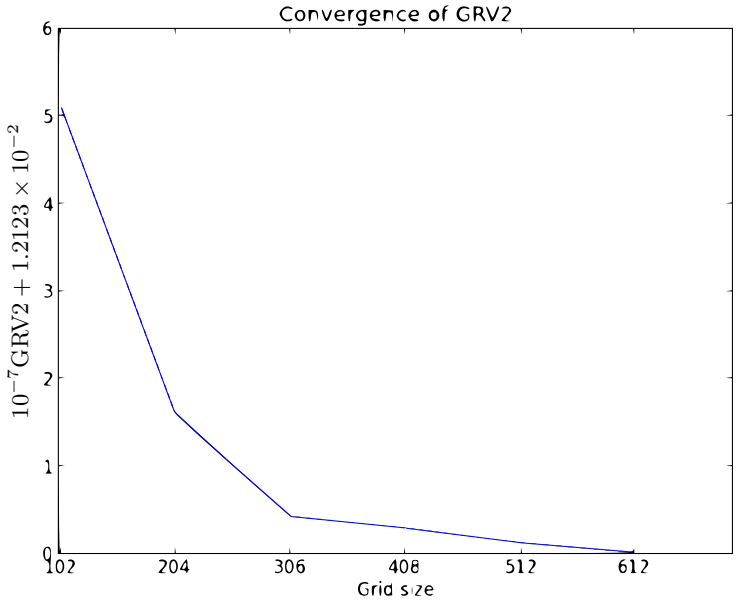

(d)

Figure 1. **(c)** Self-convergence of the numerator of λ_2 (f) in the AKM solver for increasing number of spectral coefficients. Along with (a) and (b), demonstrates the high convergence rate of spectral methods. **(d)** Convergence of GRV2 in the AKM solver for increasing number of spectral coefficients, using data output on a finite pseudo-Cartesian grid. The scale indicates the difference between the value of GRV2 calculated for n spectral coefficients, $\mathrm{GRV2}_n$, and the apparent value it converged to in this simulation, $\mathrm{GRV2}_\infty = 1.2123 \times 10^{-2}$. This particularly demonstrates the necessity of performing the calculation of GRV2 in the spectral domain, as we expect $\mathrm{GRV2}_\infty = 0$, and we note GRV2 depends on values extending to spatial infinity, which cannot be accounted for with a finite Cartesian grid.

Appendices

A Boundary Behavior in the Exterior Subdomain

In the outer subdomain, the AKM solver uses (s,t) coordinates defined from (ϱ,ζ) cylindrical coordinates as

$$\begin{aligned}\varrho_0^2(s,t) &= t\left(r_e^2 - r_p^2 + \xi^2\right)\\ \zeta_0^2(s,t) &= (1-t)\left(\xi^2 - r_p^2\right) + G(t) - r_e^2 t\\ \xi(s) &= r_p + r_e\frac{1-s}{s}\end{aligned} \tag{22}$$

To simplify the change of variables, we first change from (ϱ,ζ) to (ϱ^2,ζ^2), and then from (ϱ^2,ζ^2) to (s,t). Transforming from (ϱ,ζ) to (ϱ^2,ζ^2) space introduces the Jacobian determinant

$$|\mathbf{J}'| = \frac{1}{4\varrho_0(s,t)\zeta_0(s,t)} \tag{23}$$

to the integral. The transformation into (s,t) space then introduces the determinant

$$\begin{aligned}|\mathbf{J}_0'| &= \left(\frac{\mathrm{d}\varrho_0^2}{\mathrm{d}s}\frac{\mathrm{d}\zeta_0^2}{\mathrm{d}t} - \frac{\mathrm{d}\varrho_0^2}{\mathrm{d}t}\frac{\mathrm{d}\zeta_0^2}{\mathrm{d}s}\right)\\ |\mathbf{J}_0'| &= -\frac{2r_e(r_e(s-1)-r_p s)\left(r_e(-2r_p s(s-1)+r_e(1+2s(s-1))) - s^2 t G'(t)\right)}{s^5}.\end{aligned} \tag{24}$$

Thus the Jacobian determinant for the total transformation is

$$\begin{aligned}|\mathbf{J}_0| &= \frac{1}{4\varrho_0(s,t)\zeta_0(s,t)}\left(\frac{\mathrm{d}\varrho_0^2}{\mathrm{d}s}\frac{\mathrm{d}\zeta_0^2}{\mathrm{d}t} - \frac{\mathrm{d}\varrho_0^2}{\mathrm{d}t}\frac{\mathrm{d}\zeta_0^2}{\mathrm{d}s}\right)\\ |\mathbf{J}_0| &= -\frac{2r_e(r_e(s-1)-r_p s)\left(r_e(-2r_p s(s-1)+r_e(1+2s(s-1))) - s^2 t G'(t)\right)}{4s^5\sqrt{\left((1-t)\left(\xi^2-r_p^2\right)+G(t)-r_e^2 t\right)\left(t\left(r_e^2-r_p^2+\xi^2\right)\right)}}.\end{aligned} \tag{25}$$

Altogether then, we have the integrand

$$g_0(s,t)|\mathbf{J}_0| = \left((\nabla_{st}\nu)^2 - \frac{3}{4}\varrho_0^2(s,t)B^2 e^{-4\nu}(\nabla_{st}\omega)^2\right)|\mathbf{J}_0|. \tag{26}$$

We can simplify this equation using (19):

$$g_0(s,t)|\mathbf{J}_0| = \left((\nabla'_{st}\nu)^2 - \frac{3}{4}\varrho_0^2(s,t)B^2 e^{-4\nu}(\nabla'_{st}\omega)^2\right)|\mathbf{J}_0|^{-1}(2\varrho_0(s,t)\zeta_0(s,t))^{-2}, \tag{27}$$

where

$$(\nabla'_{st}\alpha)^2 = \varrho_0^2\left(\frac{\partial\alpha}{\partial s}\frac{\partial\zeta_0^2}{\partial t} - \frac{\partial\alpha}{\partial t}\frac{\partial\zeta_0^2}{\partial s}\right)^2 + \zeta_0^2\left(\frac{\partial\alpha}{\partial s}\frac{\partial\varrho_0^2}{\partial t} - \frac{\partial\alpha}{\partial t}\frac{\partial\varrho_0^2}{\partial s}\right)^2. \tag{28}$$

A.1 $s = 0$ Limit

For the $s \to 0$ limit, we must use L'Hopital's Rule. Expanding (27) in Mathematica, we see that its numerator and denominator both go to 0 as $s \to 0$. However, we see:

$$\lim_{s\to 0} g_0(s,t)|\mathbf{J}_0| = \lim_{s\to 0}\frac{\frac{\mathrm{d}}{\mathrm{d}s}\texttt{Numerator}[g_0(s,t)|\mathbf{J}_0|]}{\frac{\mathrm{d}}{\mathrm{d}s}\texttt{Denominator}[g_0(s,t)|\mathbf{J}_0|]} = \frac{0}{r_e^7(1-t)(-r_e^4(1-t))^{-1/2}t^{-1/2}} = 0$$

A.2 $s = 1$ Limit

The $s \to 1$ limit behaves nicely and we will not explicitly evaluate it here.

A.3 t Limits

The $t \to 0$ limit can be found by taking the limit:

$$\lim_{t\to 0}\left[g_0(s,t)|\mathbf{J}_0|\,\mathrm{d}s\,\mathrm{d}\sqrt{t}\right] = 4\sqrt{\frac{r_e(1+2s(s-1))-2r_p s(s-1)}{r_e}}\left(\left.\frac{\mathrm{d}\nu}{\mathrm{d}s}\right|_{t=0}\right)^2 \tag{29}$$

and integrating over $\mathrm{d}s\,\mathrm{d}\sqrt{t}$. However, this precludes us from taking the $t \to 1$ limit in this manner. A possible remedy could be to break up the integrand term by term and use appropriate integration parameters for each term.

References

[1] G. B. Cook, S. L. Shapiro, and S. A. Teukolsky. "Spin-up of a rapidly rotating star by angular momentum loss - Effects of general relativity". In: *APJ* 398 (Oct. 1992), pp. 203–223. DOI: 10.1086/171849.

[2] G. B. Cook, S. L. Shapiro, and S. A. Teukolsky. "Rapidly rotating neutron stars in general relativity: Realistic equations of state". In: *APJ* 424 (Apr. 1994), pp. 823–845. DOI: 10.1086/173934.

[3] Silvano Bonazzola et al. *School on spectral methods, with applications to General Relativity and Field Theory*. http://www.lorene.obspm.fr/school/. [Online; accessed 30-June-2013]. 2005.

[4] Silvano Bonazzola and Eric Gourgoulhon. "A virial identity applied to relativistic stellar models". In: *Classical and Quantum Gravity* 11.7 (1994), p. 1775.

[5] Reinhard Meinel et al. *Relativistic Figures of Equilibrium*. Cambridge University Press, 2008.

[6] T. Nozawa et al. "Construction of highly accurate models of rotating neutron stars - comparison of three different numerical schemes". In: *AAPS* 132 (Nov. 1998), pp. 431–454. DOI: 10.1051/aas:1998304. eprint: arXiv:gr-qc/9804048.

[7] M. Ansorg, A. Kleinwächter, and R. Meinel. "Highly accurate calculation of rotating neutron stars. Detailed description of the numerical methods". In: *AAP* 405 (July 2003), pp. 711–721. DOI: 10.1051/0004-6361:20030618. eprint: arXiv:astro-ph/0301173.

[8] Silvano Bonazzola et al. *Langage Objet pour la RElativite NumeriquE*. http://www.lorene.obspm.fr/index.html. [Online; accessed 30-June-2013]. 2013.